Hydrol. Earth Syst. Sci. Discuss., https://doi.org/10.5194/hess-2017-127
Manuscript under review for journal Hydrol. Earth Syst. Sci.
Discussion started: 6 June 2017
© Author(s) 2017. CC BY 3.0 License.

Hydrology and Earth System Sciences
Open Access
Discussions

Hydrological characterization of cave drip waters in a porous limestone: Golgotha Cave, Western Australia

Kashif Mahmud[1], Gregoire Mariethoz[2], Andy Baker[3], Pauline C. Treble[4]

[1]Hawkesbury Institute for the Environment, Western Sydney University, Australia
[2]Institute of Earth Surface Dynamics, University of Lausanne, Switzerland
[3]Connected Waters Initiative Research Centre, UNSW Australia, NSW, Australia
[4]Australian Nuclear Science and Technology Organisation, Lucas Heights, NSW, Australia

Correspondence to: Kashif Mahmud (k.mahmud@westernsydney.edu.au)

Abstract

Cave drip water response to surface meteorological conditions is complex due to the heterogeneity of water movement in the karst unsaturated zone. Previous studies have focused on the monitoring of fractured rock limestones that have little or no primary porosity. In this study, we aim to further understand infiltration water hydrology in the Tamala Limestone of SW Australia, which is Quaternary aeolianite with primary porosity. We build on our previous studies of the Golgotha Cave system and utilize the existing spatial survey of 29 automated cave drip loggers and a LiDAR-based flow classification scheme, conducted in the two main chambers of this cave. We find that a daily sampling frequency at our cave site optimizes the capture of drip variability with least possible sampling artifacts. Most of the drip sites show persistent autocorrelation for at least a month. Drip discharge histograms are highly variable, showing sometimes multimodal distributions. Histogram skewness is shown to relate to the wetter than average 2013 hydrological year and modality is affected by seasonality. Finally, a combination of Multi-dimensional scaling (MDS) and clustering by k-means is used to classify similar drip types based on time series analysis. This clustering reveals four unique drip regimes which agree with the flow type classification of Mahmud et al. (2016) for this site. It highlights a spatial homogeneity in drip types in one cave chamber, and spatial heterogeneity in the other, which is in concordance with our understanding of cave chamber morphology and lithology. Our hydrological classification scheme with respect to mean discharge and the flow variation, can distinguish between groundwater flow types in limestones with primary porosity, and the technique could be used to characterize different karst formations when high-frequency automated drip logger data are available. We observe little difference in the coefficient of variation (COV) between flow classification types, probably reflecting the dominance of primary porosity at this cave site, and the seasonal variations in discharge related to storage replenishment in winter followed by recession in the periods of soil moisture deficit. Moreover, we do not find any relationship between drip variability and discharge within similar flow type.

Keywords: karst aquifers, drip loggers, infiltration, cave drip water

Hydrol. Earth Syst. Sci. Discuss., https://doi.org/10.5194/hess-2017-127
Manuscript under review for journal Hydrol. Earth Syst. Sci.
Discussion started: 6 June 2017
© Author(s) 2017. CC BY 3.0 License.

Hydrology and Earth System Sciences
Open Access
Discussions

1. Introduction

Karst features in limestone are typically developed from the solutional dissolution of fractures and bedding planes in carbonate rocks (Arbel et al. 2010). Worldwide, karst regions represent significant geographical areas with potentially high rates of infiltration through fractured and karstified carbonate rocks. The most usual recharge method in karstic aquifers is the faster infiltration through the deep karstic openings (Ford and Williams 2007). Complex spatial spreading of various karst features such as solutionally widened fractures, caves and conduits, makes the monitoring and precise groundwater recharge modeling very difficult (Lange et al. 2003) and (Arbel et al. 2010). The upper part of karstified rock (the epikarst zone) has higher permeability than the underlying vadose zone (Klimchouk 2004). Therefore, infiltration into the epikarst zone is faster compared to the drainage through it, and water is kept stored in this region. This stored water in the vadose zone seeps slowly and finally emerges inside caves as infiltrating drip waters (Williams 1983).

Karstic features such as speleothems, commonly used to reconstruct paleo-environmental records, are formed due to calcite deposition from cave drip water. Therefore, the knowledge of drip water hydrology is critical to study the paleoclimatic records (Baldini et al. 2006). An early study using tipping bucket loggers formulated a relationship between maximum discharge and coefficient of variation of discharge to categorize cave discharges (Smart and Friederich (1987), for a fractured-rock limestone system with a vertical range of approximately 140 m (GB Cave, Mendip Hills, UK). They found that the drips close to the surface have extreme coefficient of variations, whereas the drips in depths have fairly constant flow rates over time, with a significant possibility of water storage in vadose zone fractures. Thus the stalagmite record resulting from slower drips may be more closely related to the karst hydrology rather than palaeoclimate (Baldini et al. 2006). Quantitative analysis of such stalagmite drip data has, in the past, used manual observations of cave drips (e.g. Baker et al 1997). However, the recent development of automatic cave drip loggers (Collister and Mattey 2008) has enabled the generation of high temporal resolution and continuous drip discharge time-series (e.g. (Jex et al. 2012), (Cuthbert et al. 2014), (Markowska et al. 2015), (Mariethoz et al. 2012)), providing new opportunities for quantitative hydrological analysis.

Here we present monitoring data from Golgotha Cave located in SW Western Australia that has been extensively monitored since 2005, with the aim of better understanding karst drip water hydrogeology and the relationship between drip hydrology and surface climate. We build on the work of Mahmud et al. (2016), which presented the largest spatial and temporal survey of automated cave drip monitoring with matrix (primary) porosity published to date. This previous study consisted of data from two large chambers within this cave, measured in the period from 2012 to 2014, using a highly spatially (29 sites in two separate chambers) and temporally (0.001 Hz, 15 min intervals) resolved dataset and developed a recharge estimation technique for caves using the drip data and flow classification techniques of Mahmud et al. (2015). Mahmud et al. (2015) performs morphological analysis of karstic features, based on ground-based LiDAR data, to identify different flow processes in karstified limestone. Based on the findings of Mahmud et al. (2016), Mahmud et al. (2015), here we investigate the relationship between drip water hydrology and cave depth, spatial location and stalactite type, and develop a hydrological classification scheme that is appropriate to high-frequency drip logger data and limestones with a primary porosity. This classification scheme is also compared with previous studies (Baker et

© Author(s) 2017. CC BY 3.0 License.

al. 1997, Smart and Friederich 1987) to examine the limitations of these previous schemes. These findings will also help better characterize and understand water movement in highly porous karst formations.

Finally we use a combination of multi-dimensional scaling (MDS) and the popular K-Means algorithm for clustering similar drip characteristics. Time series clustering has been shown to be effective in providing useful information in various domains (Liao 2005) and is implemented here to determine the degree of similarity between two drip time series. There seems to be an increased interest in time series clustering as part of the research effort in temporal data mining. The method we use here is suitable for large datasets, has been studied extensively in the past and achieves good results with minimum computational cost (Borg and Groenen 1997, Jex et al. 2012, Scheidt and Caers 2009).

2 Site Description

2.1 Studied Cave

The cave site has been explained in detail by Mahmud et al. (2016), Mahmud et al. (2015), Treble et al. (2013). Briefly, the field site, Golgotha Cave is 200 m in length and up to 25 m in width (Figure 1), is developed in Quaternary aeolianite, which consists of wind-blown calcareous sands that were deposited along the southwest coast of Australia (Brooke et al., 2014). Vadose zone water flow, and subsequent widening by ceiling collapse, formed the cave chamber. Treble et al. (2013) described the cave site as developed in the Spearwood System of the Tamala Limestone and is mantled by a variable thick layer of sand formation having depths of between 0.3 m and 3 m. Diffuse (or matrix) flow is likely to be dominant in the Tamala Limestone formation due to its high matrix porosity (Smith et al. 2012). Karst in this region is also called "syngenetic" (Treble et al. 2013) that implies processes like preferential vertical dissolution and varying morphology of the subsurface caprock. These processes may establish vadose-zone preferential flow extending to the cave ceiling, with occasional rapid delivery of percolating waters deep into the calcarenite which end up seeping through to the cave ceiling. Therefore, this young limestone formation offers various opportunities for preferential flow into the hostrock and storage within it (Brooke et al. 2014). Golgotha Cave was chosen because (a) it is located in an intensively studied karst area (e.g.,(Mahmud et al. 2016, Mahmud et al. 2015, Treble et al. 2013, Treble et al. 2016, Treble et al. 2015)), which has 9 years of manual and 3 years of automated drip water monitoring, (b) it contains actively growing speleothems, and (c) it is accessible year-round.

Based on the findings of Treble et al. (2013) and the morphological analysis of stalactite clusters by Mahmud et al. (2015), combined with the classification of drip rate data from the underlying drip sites (Mahmud et al. 2016), we determined previously that chamber 1 (Figure 1b and c) is mostly dominated by matrix flow representing water flowing down and seeping through the rock matrix, characterised by both icicle-shape and soda straw stalactites with slow drip rates of low variability. In contrast, chamber 2 (Figure 1b and d) is typically controlled by fracture and combined flow, with high drip rates that are shown to vary over time depending upon the mode of water delivery to the preferential flow system. In fracture flow, water moves along the fracture orientation, forming curtain-shape stalactites in the direction of highest fracturing. Finally, combined flow is defined as the combination of conduit, matrix and fracture flow, resulting in a circular pattern of stalactite formation.

Hydrol. Earth Syst. Sci. Discuss., https://doi.org/10.5194/hess-2017-127
Manuscript under review for journal Hydrol. Earth Syst. Sci.
Discussion started: 6 June 2017
© Author(s) 2017. CC BY 3.0 License.

Hydrology and Earth System Sciences
Discussions

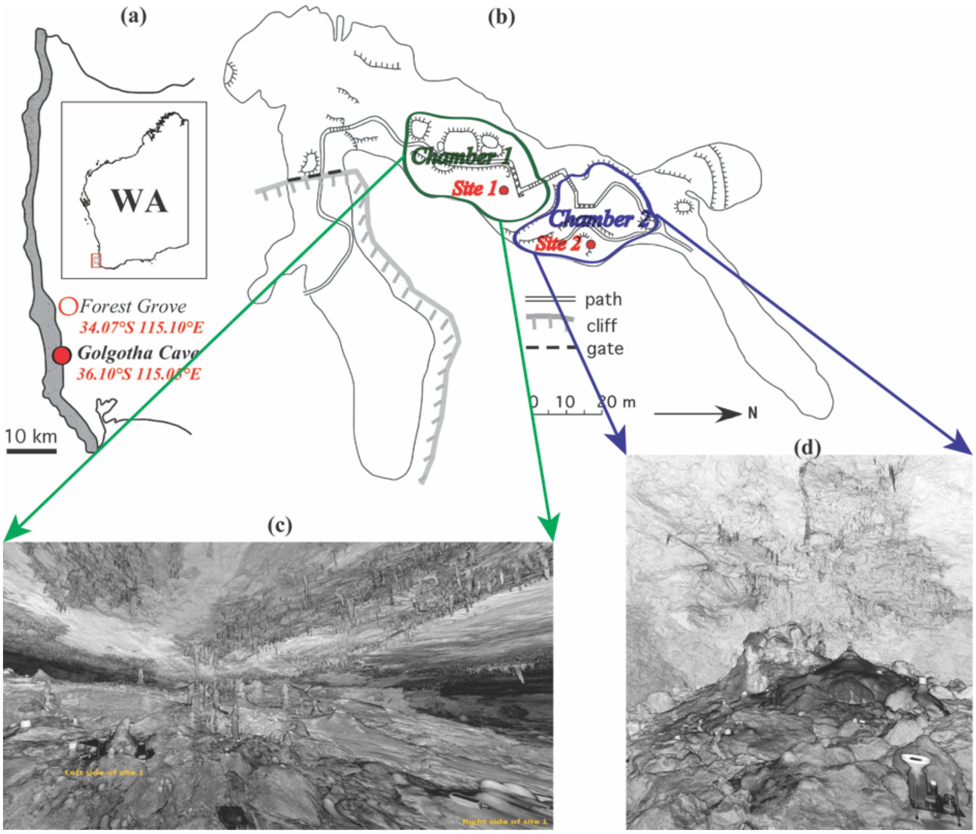

Figure 1: (a) Coastal belt of SWWA (South-West Western Australia). (b) Golgotha cave plan view displaying both Chamber 1 (green marked area), that comprises Site 1 and Chamber 2 (blue marked area) containing Site 2. Average limestone thickness from cave ceiling to ground surface over Site 1 and 2 are 32.33 m and 40.24 m respectively. (c) Site 1 LiDAR image and (d) Site 2 LiDAR image. (Fig. adapted from Mahmud et al. (2016) and Mahmud et al. (2015))

2.2 Climate and Meteorology

A comprehensive description of the climate at our study site has been presented in Mahmud et al. (2016), Mahmud et al. (2015), Treble et al. (2013). To summarize, the site is in Mediterranean climate, associated with wet winters and dry summers. Annual rainfall recorded at Forest Grove weather station (Figure 1A, 5 km away from the study site) is 1136.8 ± 184 mm, among which ~75% occurs between May and September, with an average daily maximum temperature variation from 16°C (in July) to 27°C (in February) (BoM 2015). Typically, the peak rainfall begins in late autumn (May) and the wet season continues until end of September with a median monthly rainfall of ~100 mm (Figure 2). Weekly rainfall data are shown in Fig. 2a for three hydrological years. Each hydrological year is defined as April to March, as April has the lowest water budget.

As reported in Mahmud et al. (2016), hydrological year 2012 had roughly similar annual rainfall of 1008.6 mm to the long-term annual mean, whereas 2013 was rather wet (total rainfall of 1239.8 mm) and 2014 was a relatively dry year with a total rainfall of 943.8 mm. Recorded rainfall was significantly above average in the 2013 hydrological year for various weather stations in Western Australia (BoM 2015). Therefore, our site had a wetter winter in 2013 (Fig. 2b) with an estimated annual recharge of 858.67 mm which is very much above average (ten year mean annual recharge is 564 mm).

We use the Australian Water Availability Project (AWAP) precipitation (P) and modelled evapotranspiration (ET) data to estimate both cumulative water budgets and total infiltration from April 2012 to March 2015 (Raupach et al. 2009). Weekly calculated ET was subtracted from the weekly rainfall totals to determine the weekly water budget (Figure 2a). Annual infiltration is estimated by summing all positive weekly water budgets and a smooth spline interpolation trend is plotted through those points (Figure 2a, pink line). All hydrological years have water deficit during the dry season (October to April) and significant infiltration during the wet period (Figure 2a). Low evaporative conditions during winter should permit increased infiltration to the caves, enhancing the drip discharge response to winter rainfall.

3 Drip data acquisition and characteristics

Data acquisition and pre-processing has been previously described in Mahmud et al. (2016) and is concisely summarized here. Stalagmate drip loggers (www.driptych.com) were set up in approximate transects throughout the two large chambers from higher to lower ceiling elevation in 34 locations and are currently being monitored since August 2012. Each chamber has contrasting discharge, dune facies and karst features of Golgotha Cave (Figure 3). Data loggers were set to record continuously at 15 minute intervals. The notation used for site identification follows the same style as described in Mahmud et al. (2016), consisting of a numerical number (represents the chamber) and a letter/roman number (represents a drip site within the given chamber, with a letter indicates the sites having both manual and automatic drip counts and a roman number specifies the sites only having drip logger data).

Based on the initial data screening of Mahmud et al. (2016), we entirely discard five drip sites i.e. 1iv, 1vii, 1xii, 2ii and 2xii. We observe that some of these drip sites (1iv, 2ii and 2xii) contain abrupt changes in drip rate and that is probably not recording an actual change in discharge, rather due to the logger being accidentally moved or misaligned. Some other loggers (1vii and 1xii) were removed part way through the monitoring period due to either recording dual drips or a ceasation of dripping and ignored in full. The rest of the 29 sites are considered in the time series analysis although short periods of poor quality data were omitted if they were associated with changes in the mean and variability at the time of fieldwork. This impacted sites 1A, 1B, 2A, 2B, 2E as the logger was temporarily placed aside every 6 weeks in order to sample water from a collection bottle underneath the logger. Time series gaps are filled with synthetic data based on the drip statistics and correlation between drip rates. The processed drip rate time series for all the sites and three hydrological years from April 2012 to March 2015 are plotted in Figure 2c-f.

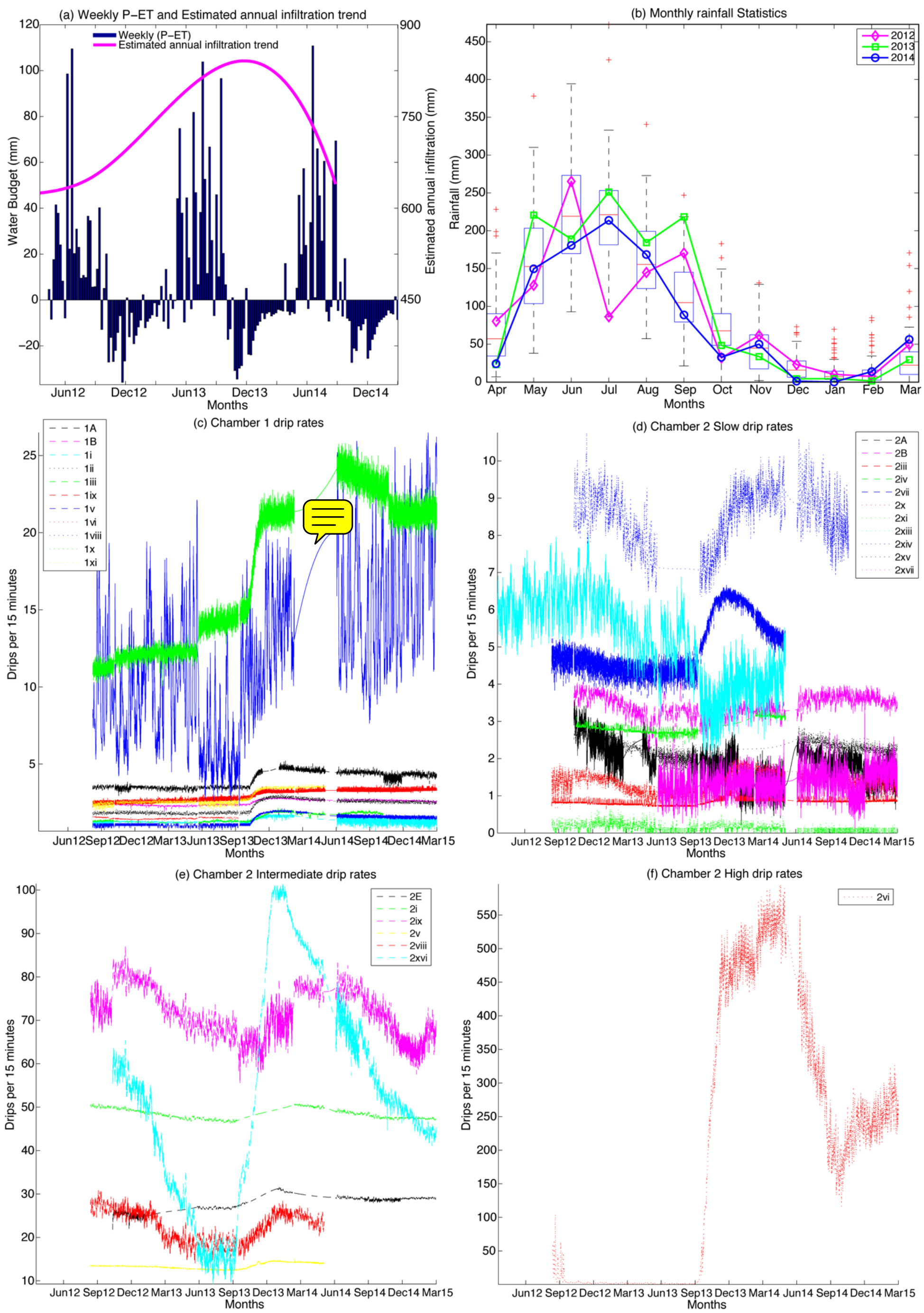

160

161 Figure 2: (a) Weekly water excess data for three hydrological years with estimated annual infiltration pattern.
162 (b) Box plot of monthly rainfall at Golgotha Cave site, (c) Chamber 1 drip rates time series. Further

Hydrology and Earth System Sciences
Discussions

classification of Chamber 2 drip sites for effective time series visualization: (d) slow flow rates with drip frequency of less than 10 drops per 15 mins, (e) medium discharges with drip frequency of between 10 to 100 drops per 15 mins, and (f) fast drip rates of more than 100 drops per 15 mins. (Fig. is adapted from Mahmud et al. (2016)).

Drip rates were also measured manually at five different sites (the location of Sites 1A, 1B, 2A, 2B and 2E shown in Figure 3) within both chambers at 4-6 week intervals using a stopwatch since 2005, however such measurements were superseded in May 2014 by the Stalagmate loggers (Treble et al. 2013). Sites 1A and 1B are located ~60 m into the cave and are approximately 0.5 m apart. Sites 2A, 2B and 2E are located ~30 m further into the cave in Chamber 2. Site 2E is located in the wettest area close to the lowest point at which the ceiling and wall intersect, whilst 2B and 2A are located on each transect, approximately 5-6 m from Site 2E. A surface soil auger survey by Treble et al. (2013) at points immediately above Chamber 2 revealed that soil depth was particularly deep above this area, which could reflect the presence of a soil-filled doline-type structure. We use these available manual drip data for quality assurance of loggers automatic drip rates for the two hydrological years (August 2012 to May 2014). Drip rates recorded by the loggers tend to match the manual data for these drip sites, with slight variations in absolute value between manual and logger data for the slow dripping sites due to 15 minutes sampling intervals.

Drip rates in Chamber 1 are generally very low (the fastest drip rate was 25 drips per 15 mins) consistent with the predominance of matrix flow in this chamber. However, it is obvious that most drip loggers exhibit a clear response to the 2013 wet winter, presenting peak discharges at the end of September 2013 (Figure 2) and also indicate the substantial inter-annual variation in discharge between three hydrological years. All chamber 1 drip sites (except site 1x) show a gradual drip rate decrease during summer 2012 to winter 2013 due to below average rainfall in 2012 that produces high water deficit (Figure 2). Then after displaying the sudden increase in all drip discharges that express the 2013 wet winter, the drip rates further reduce due to the dry 2014 hydrological year. This intra-annual variation is identified much greater than the inter-annual discharge variation of the drip sites, as previously observed in Baker et al. (1997). This suggests that high-resolution intra-annual drip rate data is helpful to obtain a complete picture of changing flow variability with recharge. The high resolution of the data sets includes precise characterization of the temporal behavior of an individual drip, illustrating the differences inherent to the drip sites.

In contrast, Chamber 2 drip rates present more variability between sites both in intra-annual and inter-annual discharges, except few very slow dripping sites (Figure 2d). To envisage the drip time series efficiently, they were further divided into three classes on the basis of their flow behavior through the three-year study period (Mahmud et al. 2016): (i) slow drips with little discernable variation through time and very low flow rates (Figure 2d), (ii) medium-variability drips with moderate discharges (Figure 2e), and (iii) high-variability drips with high discharges (Figure 2f).

Of the Chamber 2 drips, the slow drip sites have the lowest COVs and lowest discharges (Figure 2d), indicative of matrix flow types (Mahmud et al., 2016). Drip rates at intermediate sites (Figure 2e) are considerably greater (typically ×10) than those of slow dripping sites (Figure 2d). The drip site 2vi has the maximum discharge from all drip sites, with 550 drips per 15 mins peaking in response to the wet 2013 winter (Figure 2f). The timing of

© Author(s) 2017. CC BY 3.0 License.

maximum drip rates is generally delayed in Chamber 2 versus Chamber 1: Chamber 1 drip rates typically peak in late spring/early summer (Oct-Dec) while Chamber 2 drips tend to peak a few months later (Dec-May), reflecting a longer water residence time (Figure 2c-f). This may be a function of the thicker ceiling above Chamber 2 (40.24 versus 32.33 m) but also heterogeneity in flowpaths to each chamber (Mahmud et al., 2015; Treble et al., 2016). Overall the drip response to the 2013 wet winter is amplified in Chamber 2 versus Chamber 1, consistent with the presence of greater fracture flow in Chamber 2 (Mahmud et al., 2015).

Hydrol. Earth Syst. Sci. Discuss., https://doi.org/10.5194/hess-2017-127
Manuscript under review for journal Hydrol. Earth Syst. Sci.
Discussion started: 6 June 2017
© Author(s) 2017. CC BY 3.0 License.
Hydrology and Earth System Sciences
Discussions
Open Access

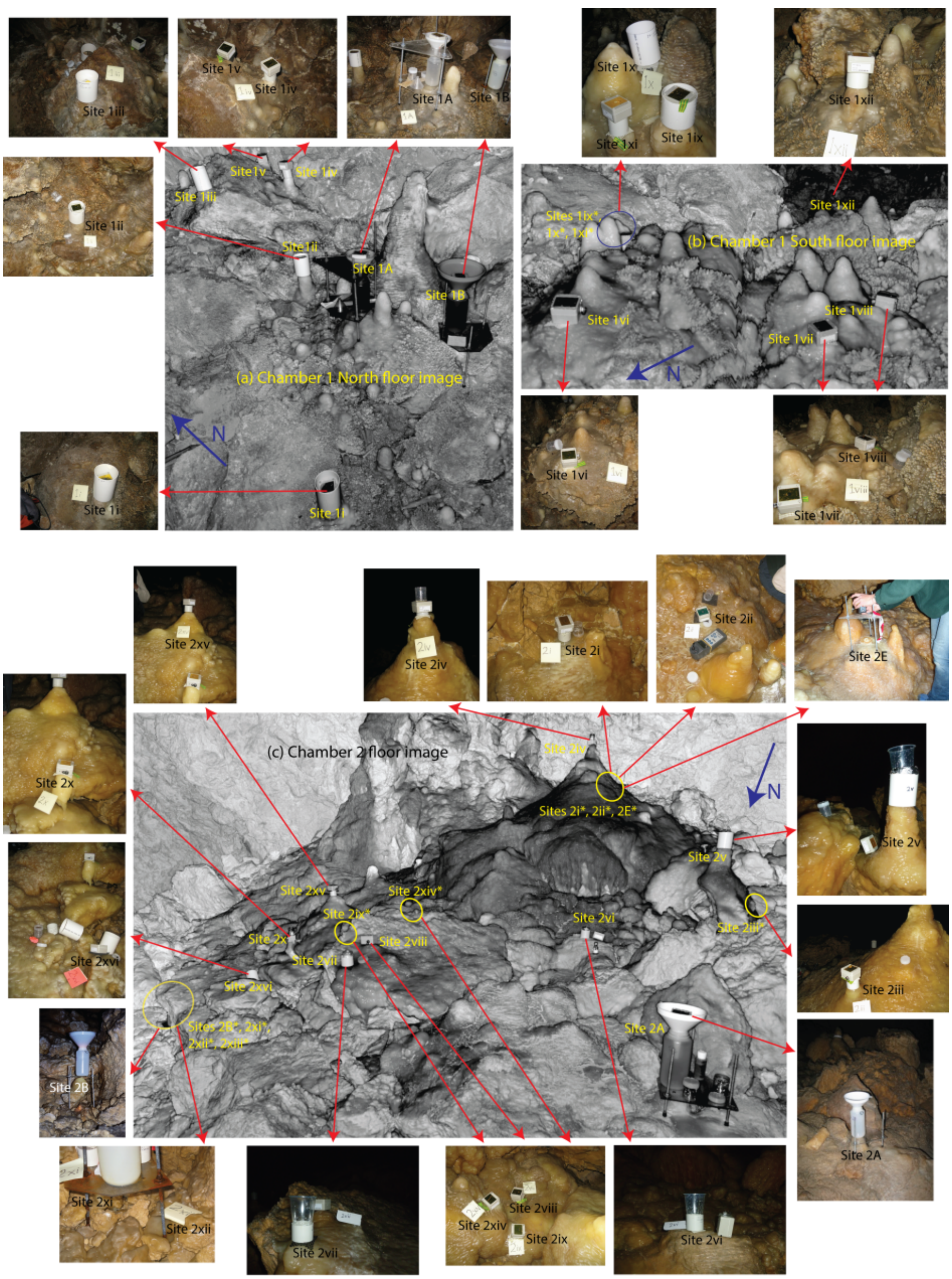

Figure 3: LiDAR images of drip sites on floor plus photographs of underlying stalagmites. The blue arrows in all Figures show the geographic orientation. * indicates the sites where the stalagmate loggers are not clearly visible in the LiDAR floor images as they are obscured by formations in front of them, however the rough

© Author(s) 2017. CC BY 3.0 License.

locations are marked in yellow circles. Complimentary image of cave ceiling are shown in Fig. 3 of Mahmud et al. (2016).

4 Clustering of similar drip time series

One key component in clustering is the function used to measure the temporal similarity (or distance) between any two time series being compared. To define an appropriate measure of similarity between time series, we determine two factors: firstly the offset (*O*) to match two time series based on their maximum correlation, and secondly the complement of the correlation coefficient (1-*R*) between the time series (Jex et al. 2012). Initially, we compute the cross-correlation function and *O* is defined as the lag time based on the maximum correlation between two time series. Next we define *R* as the correlation coefficient with the time series being moved by the offset amount *O* to have maximum correlation coefficient. Finally the distance matrix (*d*) is computed for each pair of loggers using the following equation (Jex et al. 2012):

$$d = O\,(1 - R)$$

Next, MDS is used to translate these distances into a configuration of points defined in an n-dimensional Euclidean space (Borg and Groenen 1997, Cox and Cox 1994). A MDS results in a set of points arranged so that their corresponding Euclidean distances indicate the dissimilarities of the time series. The K-Means clustering algorithm is then used to divide these points into k clusters, which corresponds to a categorization of the drip data time series. Here we use 4 clusters as this was the number of flow categories identified by Mahmud et al. (2016).

5 Results and Discussion

The statistical properties of the drip data (skewness, COV), elevation and LiDAR classified flow type are taken from Mahmud et al. (2016), Mahmud et al. (2015) are listed in Table 1 and Table 2. Average drip discharges are calculated from the 15-minute drip rates that appear in Tables 1 and 2 of Mahmud et al (2016). The MDS cluster groups (analyzed later in section 5.4) are also listed in Table 1 and Table 2.

Table 1: Statistical properties of chamber 1 drip data

Site/Stalagmate	Elevation (ASL m)	Average drip discharge (l/yr)	Skewness	COV	Flow type	**MDS Cluster Group**
	(Mahmud et al. 2016)					
1A	77.46	19.8	0.17	18.23	Icicle	**1**
1B	77.424	12.6	-0.03	19.93	Icicle	**1**
1i	77.4	6.6	0.13	40.31	Icicle	**1**
1ii	77.521	11.2	-0.06	28.09	Icicle	**1**
1iii	77.655	8.1	-0.29	30.52	Icicle	**1**
1v	77.585	6.7	1.21	40.83	Soda-straw	**1**
1vi	77.036	7.4	0.1	33.83	Icicle	**1**
1viii	77.167	60.9	0.38	42.49	Combined	**2**
1ix	76.88	14.8	0.23	21.01	Icicle	**1**
1x	76.9	86.2	0.19	28.88	Fracture	**3**
1xi	76.885	12.7	-0.71	48.98	Icicle	**1**

© Author(s) 2017. CC BY 3.0 License.

Table 2: Statistical properties of chamber 2 drip data

Site/Stalagmate	Elevation (ASL m)	Average drip discharge (l/yr)	Skewness	COV	Flow type (Mahmud et al. 2016)	**MDS Cluster Group**
	(Mahmud et al. 2016)					
2A	75.48	9.4	-0.24	44.31	Icicle	**1**
2B	73.49	17.1	0.2	16.01	Icicle	**1**
2E	75.37	140.3	-0.59	6.21	Combined	**3**
2i	72.22	243.0	0.31	2.57	Fracture	**4**
2iii	75.2	4.2	-1.64	45.62	Soda-straw	**1**
2iv	73.7	14.6	-0.82	13.23	Icicle	**1**
2v	75.75	67.8	0.10	5.65	Combined	**3**
2vi	75.66	985.0	0.44	100.95	Fracture	**1**
2vii	75.7	25.0	0.03	21.63	Icicle	**2**
2viii	73.72	113.8	-0.11	16.11	Combined	**3**
2ix	73.34	360.2	-0.22	8.3	Fracture	**4**
2x	73.59	7.0	0.5	43.86	Icicle	**1**
2xi	73.5	0.6	2.68	289.31	Soda-straw	**1**
2xiii	73.54	26.2	-0.47	25.29	Icicle	**2**
2xiv	73.49	42.8	-0.17	11.81	Icicle	**2**
2xv	73.36	11.6	0.56	21.57	Icicle	**1**
2xvi	73.52	266.9	0.17	45.28	Fracture	**3**
2xvii	73.72	7.0	-0.06	53.08	Icicle	**1**

5.1 Histogram plots

We plot drip rate histograms for representative drip sites in Figure 4 for different flow categories. Drip sites are organized from lowest to highest discharge in each flow classification (Mahmud et al. 2016). All of the slow dripping soda straw types typically fall into two bins only. The lower drip counts (sites 2iii, 1v) indicate the drip response of hydrological years 2012 and 2013 until the wet winter, and the higher values direct the consequence of the infiltration due to high rainfall events during the entire 2013 winter (April - September). The histograms for icicle flow types show unimodal normal distribution, while the combined flow systems represent bimodal distributions. The rest of the fracture sites show bimodal or multimodal distributions. With the limited temporal scale of the analysis, it seems that the histograms with skewed distribution (sites 1xi, 2vii, 2xiii, 2xiv) actually represent the wetter 2013 hydrological year. In contrast, the bimodal distributions indicate the drip response to the annual cycle of wet and dry seasons of each hydrological year.

© Author(s) 2017. CC BY 3.0 License.

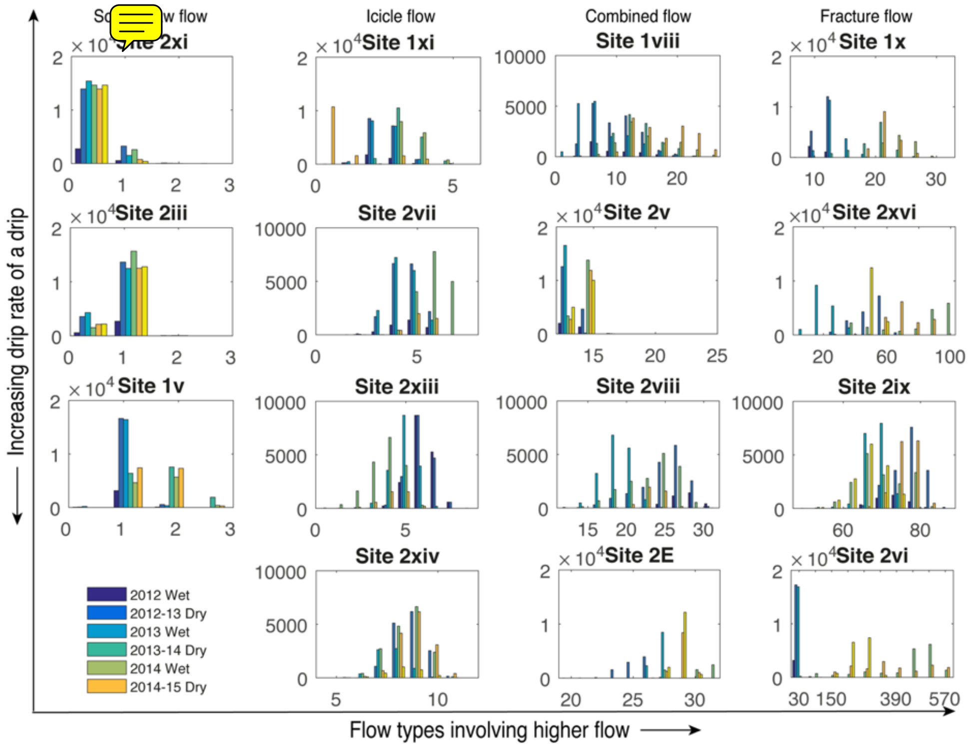

Figure 4: Histogram plots of both chambers drip data according to four flow types identified by Mahmud et al. (2016). The histogram represents the frequency of the drip counts per 15 minutes. Note that the bin size is variable because the unit is in drips per 15 minutes and slow drips only take a small number of discrete values, in contrast to fast drips for which we can see the entire distribution, including multimodality. The legend shows all the seasons over the monitoring period (wet seasons: April to September and dry seasons: October to March). 2012 wet season had similar to long-term annual mean rainfall event, whereas 2013 was rather wet and 2014 was a relatively dry year.

5.2 Autocorrelation functions

We plot autocorrelation functions (ACF) for major drip sites in Figure 5 for different flow categories using the optimum sampling frequency of 1-day (see next section). All sites have an autocorrelation that persists for at least a month, and often much longer. However, there is no relationship between the strength of correlation or the time period of the autocorrelation and the flow type. This indicates the presence of ample storage in the system, supplying all stalactite types.

© Author(s) 2017. CC BY 3.0 License.

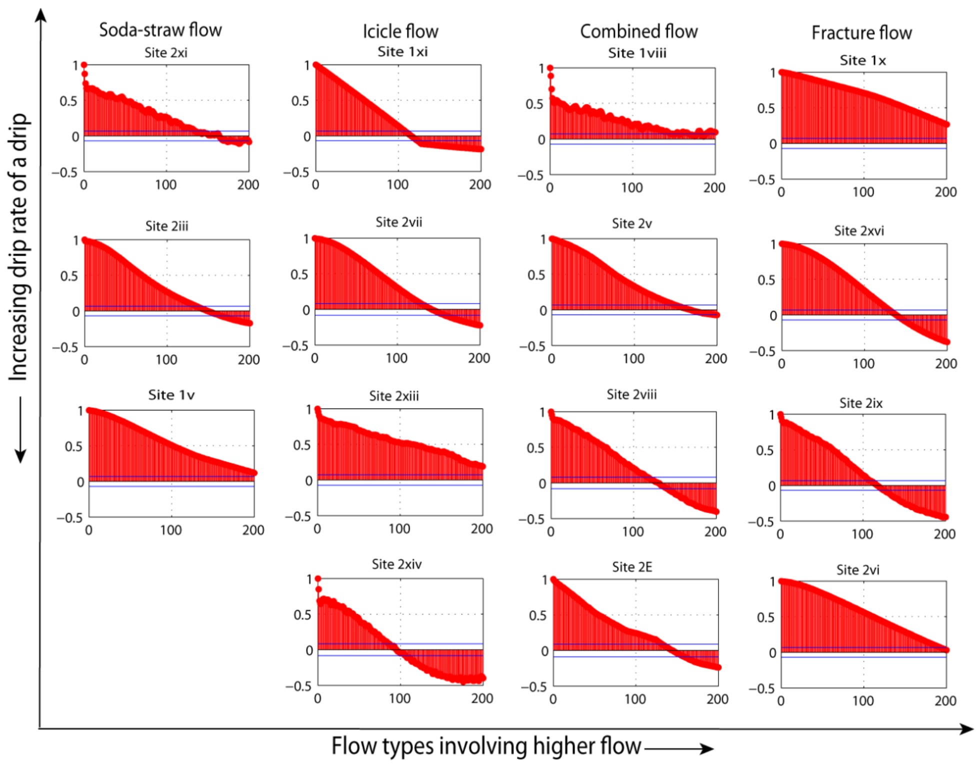

Figure 5: Autocorrelation functions of both chambers drip data according to flow classification of Mahmud et al. (2016). X- and Y-axis of individual plots represents the lag (in days) and ACF respectively.

5.3 Hydrological classification of cave drips

Research involving automated drip monitoring systems is increasing, for example at Cathedral Cave in Wellington (Cuthbert et al. 2014) and Harrie Wood Cave in Snowy Mountain, Yarrangobilly (Markowska et al. 2015). The variability of the drip discharge might not only be a function of discharge itself, but might also depend on the sampling frequency. We investigate this possibility in Figure 6 that shows COV versus sampling interval, calculated by resampling the data. Figure 6 shows that for high discharge, COV increases with sampling frequency, which we explain by the smaller sampling interval better capturing the actual drip variability. For low discharges, COV also increases with sampling frequency, which we explain by the variability introduced due to drip rates being less than the sampling frequency. From the data presented in Figure 6, we can conclude that for both chambers and different types of flow, a sampling frequency of 1 day gives the minimum COV, which does not change significantly with a finer sampling frequency. Therefore, we use a sampling frequency of 1 day that minimizes sampling artifacts while maximizing the capture of natural variability. For Golgotha Cave, this would be to sum the 15 minutes drip rates over a 1-day period. Using this optimum sampling frequency of 1-day, we summarize the mean discharge of drip sites in relation to the variability in discharge in

© Author(s) 2017. CC BY 3.0 License.

Figure 7. These are the same drip discharge parameters as used in the classification method proposed by Friederich and Smart (1982), Fairchild et al. (2006) and Baker et al. (1997) that were based on manual drip collection at low frequency.

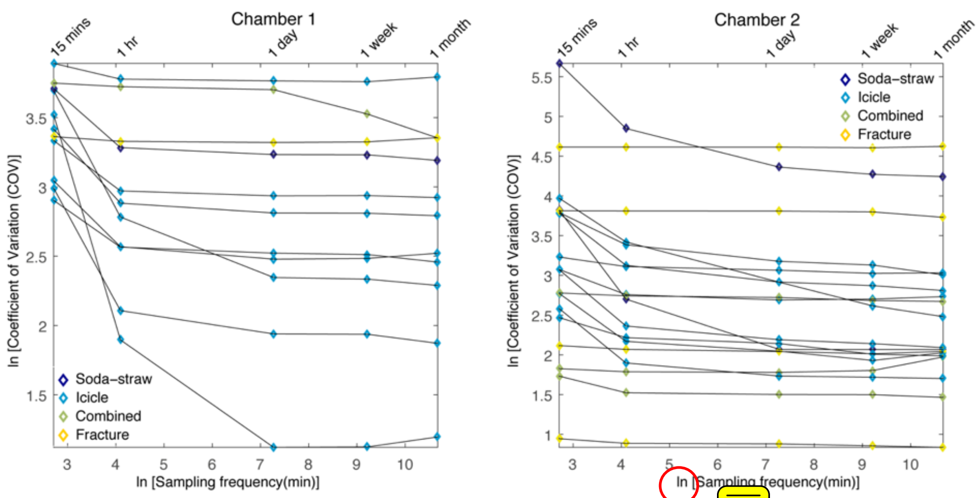

Figure 6: Optimum sampling frequency that minimizes sampling artifacts while maximizing the capture of natural variability.

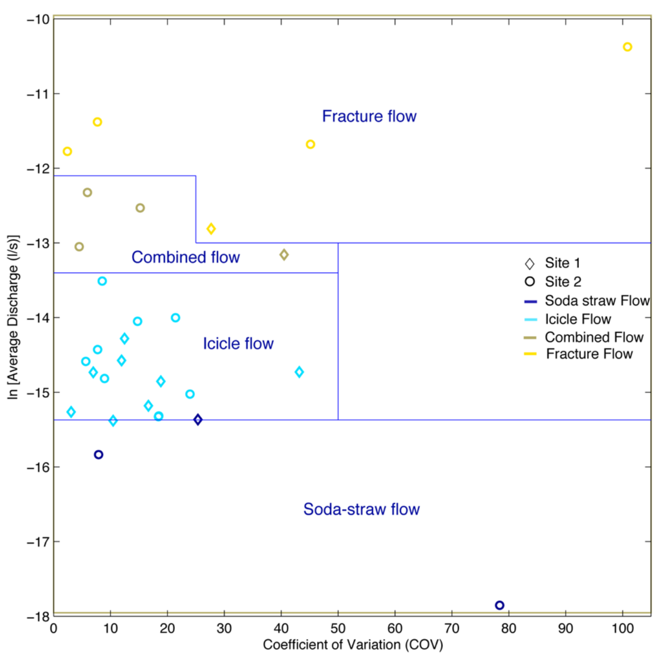

Figure 7: Hydrological behaviour of drip sites expressed in terms of daily mean discharge versus daily discharge variability calculated from the automatic drip rate data for three hydrological years. Measured drip rates are

Hydrol. Earth Syst. Sci. Discuss., https://doi.org/10.5194/hess-2017-127
Manuscript under review for journal Hydrol. Earth Syst. Sci.
Discussion started: 6 June 2017
© Author(s) 2017. CC BY 3.0 License.
Hydrology and Earth System Sciences
Discussions

converted to volume units assuming a drip volume of 0.1433 ml (Genty and Deflandre 1998). Blue lines reflect flow classification given in Mahmud et al. (2015).

We examine the hydrological behavior of the drips at daily resolution with respect to mean discharge and the flow variation in

Figure 7. This classification scheme shows that Golgotha Cave drip sites do not fit within the drip classification method proposed by Smart and Friederich (1987) and Baker et al. (1997), which were based on manual drip counts with low frequency and limited number of drip sites. It is clear from

Figure 7 that there is a broad continuum from soda-straw flow to fracture flow. One soda-straw discharge (site 2xi) has a seasonal dryness, a very low discharge, and a very high coefficient of variation due to its intermittent dripping. Otherwise, nearly all soda-straw flow, icicle flow and combined flow drips have COV <60%, whereas fracture flow has a greater COV range, up to 100%. But in general, there is little difference in the COV between classification types, probably reflecting the dominance of primary porosity at this cave, and the seasonal variations in discharge related to storage replenishment in winter followed by recession in the periods of soil moisture deficit. We do not clearly observe increasing variability with decreasing discharge within similar flow type, in contrast to other studies from older, fractured rock limestones (Baker et al. 1997, Baldini et al. 2006, Smart and Friederich 1987).

5.4 Clustering of similar drip time series

The clustering results are overlain upon the chamber ceiling images in Figure 8 and also summarized in Tables 1 and 2. As mentioned above, drip logger time series are deemed similar if they are well correlated and only have a small offset with each other, and so these time series should cluster together. Most of the drip sites that are identified as matrix flow (soda-straw and icicle flow) cluster together in C1. However, three of the icicle flow sites with drip rate greater than 4 per 15 minutes fall in C2. The combined flow category and the fracture type usually cluster in C3 and C4 respectively. Therefore we observe that our clustering generally agrees with the morphology-based flow classification of Mahmud et al. (2016). Few of the flow classes show exceptions, for example site 2vi is a fracture type flow and cluster in C1. This site has really high discharge but low variability in terms of drip rate and shows inconsistency.

One consistent feature that appears from the cluster analysis of Figure 8 is the spatial homogeneity of the clusters in Chamber 1, suggesting that they are spatially connected and supporting the overall dominant matrix flow (both soda-straw and icicle) patterns. However, a completely different situation is demonstrated for Chamber 2. From Chamber 2, it is obvious that drip sites can have similar behavior (well correlated together with a small lag), and be spatially distinct features, separated by spans of approximately 6m (Figure 8). In particular, cluster 3 and 4 are spatially scattered, representing the presence of fractures and combined flow systems throughout the chamber ceiling. This indicates an overall strong heterogeneity of the flow paths between the surface and the cave for Chamber 2. Hence in Chamber 2, we expect flow paths to be more complex with potential routing between multiple stores and interconnected fracture networks potentially

© Author(s) 2017. CC BY 3.0 License.

resulting in non-linear response to infiltration. This is supported by dripwater $\delta^{18}O$ data for this chamber (Treble et al. 2013).

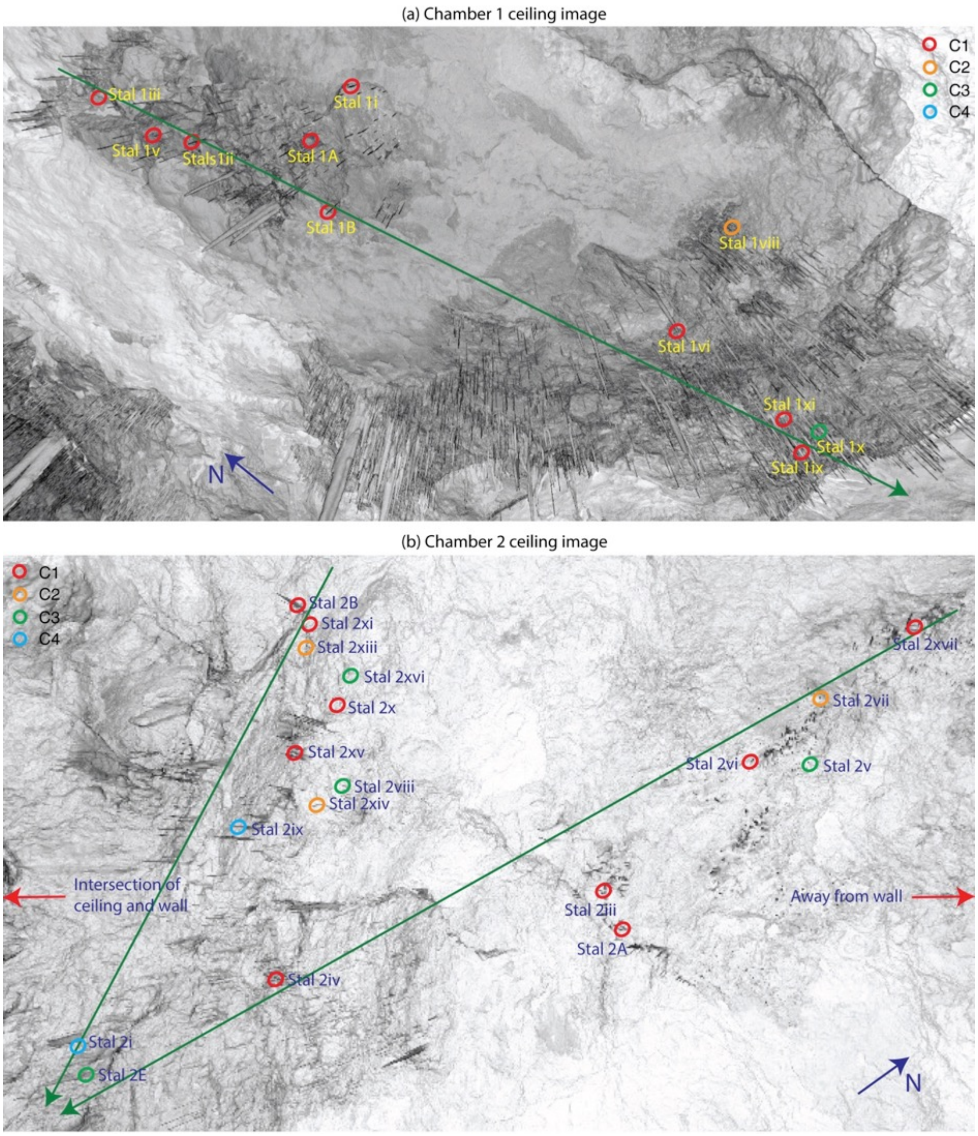

Figure 8: Cluster group plot overlain upon the cave ceiling for both chambers. The ceiling images are captured by LiDAR and the circles represent the ceiling locations of stalactites dripping on various stalagmates in both chambers (shown in Figure 3). The colour of the circles indicates individual MDS cluster group. The blue arrows in both Figures show the geographic orientation and the green arrows represent the approximate transects throughout the chambers from higher to lower ceiling elevation.

© Author(s) 2017. CC BY 3.0 License.

6 Conclusion

Cave drip water response to surface climatic conditions is often complex due to numerous interacting drip routes with varying response times (Baldini et al. 2006). This study explores the relationship between drip water and rainfall in a SW Australian karst, where both intra- and inter-annual hydrological variations are strongly controlled by seasonal variations in recharge. Building on the studies of Mahmud et al. (2015) and Mahmud et al. (2016), we further analyse a set of statistical properties of three hydrological years of drip data under varying precipitation rates. The histogram distributions of various drip data time series illustrate a relationship between the flow classification and surface infiltration. Moreover, we test the relationship between drip discharge variability and drip data sampling frequency to determine the optimum sampling frequency that maximizes the capture of natural variability with minimum sampling artifacts. Using the daily optimum sampling frequency, most of the drip sites show persistent autocorrelation for at least a month.

The hydrological behavior of the drips is examined at daily resolution with respect to mean discharge and the flow variation is similar to the classification method proposed by previous researchers (Baker et al. 1997, Baldini et al. 2006, Smart and Friederich 1987). The drip sites at Golgotha Cave described in this study do not fit within the drip classification method proposed by Smart and Friederich (1987) and Baker et al. (1997). These previous studies were based on manual drip counts with low frequency and limited number of drip sites. Here we overcome these limitations with high frequency drip signals.

Finally, we apply a well-developed clustering method to determine the degree of similarity between drip time series. The clustering indicates one dominating group: C1 (characterized by matrix flow type) with very slow continuous drip discharge indicating matrix porosity in the thick limestone formation. This finding concurs with the observed cave chamber morphology and lithology. Moreover, the cluster analysis agrees with the flow classification of Mahmud et al. (2016) by grouping similar flow type in one single cluster.

Over the last decade, the automation of cave drip water hydrology measurements has permitted the routine generation of continuous hydrological time series for the first time. This study demonstrates a complete methodology for such datasets, which will help better characterize karst drip water hydrogeology and understand the relationship between drip hydrology and surface climate at any cave site where such measurements are made. We demonstrate that the analysis of the time series produced by cave drip loggers generates useful hydrogeological information that can be applied generally, beyond the example presented here. The time series behaviour integrates a variety of characteristics that combine the properties of the epikarst (storage), fracture configuration, and recharge. The clustering approach can identify which drip behaviour are related to these cave characteristics, and their spatial relationship. Most importantly, information on cave characteristics can now be gathered at a very low cost in terms of measurement and time.

Acknowledgment

This paper is based on work supported by UNSW Australia, UNSW Connected Waters Initiative Research Center and the National Centre for Groundwater Research and Training. The authors wish to thank individuals

© Author(s) 2017. CC BY 3.0 License.

(Andy Spate, Alan Griffiths, Liz McGuire, Carolina Paice, Anne Wood and others) who assisted in data acquisition at Golgotha cave site.

References

Arbel, Y., Greenbaum, N., Lange, J. and Inbar, M. (2010) Infiltration processes and flow rates in developed karst vadose zone using tracers in cave drips. Earth Surface Processes and Landforms 35(14), 1682-1693.

Baker, A., Barnes, W.L. and Smart, P.L. (1997) Variations in the discharge and organic matter content of stalagmite drip waters in Lower Cave, Bristol. Hydrological Processes 11(11), 1541-1555.

Baldini, J.U.L., McDermott, F. and Fairchild, I.J. (2006) Spatial variability in cave drip water hydrochemistry: Implications for stalagmite paleoclimate records. Chemical Geology 235(3–4), 390-404.

BoM (2015) Climate Data Online (Station 9547), Bureau of Meteorology Melbourne. http://www.bom.gov.au/climate/data/ (Accessed 26-08-2014).

Borg, I. and Groenen, P. (1997) Modern multidimensional scaling: theory and applications, Springer, New York.

Brooke, B.P., Olley, J.M., Pietsch, T., Playford, P.E., Haines, P.W., Murray-Wallace, C.V. and Woodroffe, C.D. (2014) Chronology of Quaternary coastal aeolianite deposition and the drowned shorelines of southwestern Western Australia – a reappraisal. Quaternary Science Reviews 93, 106-124.

Collister, C. and Mattey, D. (2008) Controls on water drop volume at speleothem drip sites: An experimental study. Journal of Hydrology 358(3–4), 259-267.

Cox, T. and Cox, M. (1994) Multidimensional scaling, Chapman and Hall, London.

Cuthbert, M.O., Baker, A., Jex, C.N., Graham, P.W., Treble, P.C., Andersen, M.S. and Ian Acworth, R. (2014) Drip water isotopes in semi-arid karst: Implications for speleothem paleoclimatology. Earth and Planetary Science Letters 395, 194-204.

Fairchild, I.J., Tuckwell, G.W., Baker, A. and Tooth, A.F. (2006) Modelling of dripwater hydrology and hydrogeochemistry in a weakly karstified aquifer (Bath, UK): Implications for climate change studies. Journal of Hydrology 321(1–4), 213-231.

Ford, D. and Williams, P. (2007) Karst Hydrogeology and Geomorphology, Wiley.

Friederich, H. and Smart, P.L. (1982) The classification of autogenic percolation waters in karst aquifers: A study in G.B. cave, Mendip Hills, England, pp. 143–159.

Genty, D. and Deflandre, G. (1998) Drip flow variations under a stalactite of the Pere Noel cave (Belgium). Evidence of seasonal variations and air pressure constraints. Journal of Hydrology 211(1-4), 208-232.

Jex, C.N., Mariethoz, G., Baker, A., Graham, P., Andersen, M., Acworth, I., Edwards, N. and Azcurra, C. (2012) Spatially dense drip hydrological monitoring and infiltration behaviour at the Wellington Caves, South East Australia. International Journal of Speleology 41(2), 283–296.

Klimchouk, A. (2004) Towards defining, delimiting and classifying epikarst: Its origin, processes and variants of geomorphic evolution. Speleogenesis and Evolution of Karst Aquifers 2(1), 1-13.

Lange, J., Greenbaum, N., Husary, S., Ghanem, M., Leibundgut, C. and Schick, A.P. (2003) Runoff generation from successive simulated rainfalls on a rocky, semi-arid, Mediterranean hillslope. Hydrological Processes 17(2), 279-296.

© Author(s) 2017. CC BY 3.0 License.

Liao, T.W. (2005) Clustering of time series data-a survey. Pattern Recogn. 38(11), 1857-1874.

Mahmud, K., Mariethoz, G., Baker, A., Treble, P.C., Markowska, M. and McGuire, L. (2016) Estimation of deep infiltration in unsaturated limestone environments using cave LiDAR and drip count data. Hydrol. Earth Syst. Sci. 20, 359-373.

Mahmud, K., Mariethoz, G., Pauline, C.T. and Baker, A. (2015) Terrestrial Lidar Survey and Morphological Analysis to Identify Infiltration Properties in the Tamala Limestone, Western Australia. Selected Topics in Applied Earth Observations and Remote Sensing, IEEE Journal of 8(10), 4871 - 4881.

Mariethoz, G., Baker, A., Sivakumar, B., Hartland, A. and Graham, P. (2012) Chaos in karst percolation. Geophysical research letters 39(L23305).

Markowska, M., Baker, A., Treble, P.C., Andersen, M.S., Hankin, S., Jex, C.N., Tadros, C.V. and Roach, R. (2015) Unsaturated zone hydrology and cave drip discharge water response: Implications for speleothem paleoclimate record variability. Journal of Hydrology 529(2), 662–675.

Raupach, M.R., Briggs, P.R., Haverd, V., King, E.A., Paget, M. and Trudinger, C.M. (2009) Australian Water Availability Project (AWAP): CSIRO Marine and Atmospheric Research Component: Final Report for Phase 3, p. 67.

Scheidt, C. and Caers, J. (2009) Representing spatial uncertainty using distances and kernels. Mathematical Geosciences 41(4), 397-419.

Smart, P.L. and Friederich, H. (1987) Water movement and storage in the unsaturated zone of a maturely karstified carbonate aquifer, pp. 59-87, Natural Water Well Association, Dublin, Ohio.

Smith, A.J., Massuel, S. and Pollock, D.W. (2012) Geohydrology of the Tamala Limestone Formation in the Perth Region: Origin and Role of Secondary Porosity, p. 63.

Treble, P.C., Bradley, C., Wood, A., Baker, A., Jex, C.N., Fairchild, I.J., Gagan, M.K., Cowley, J. and Azcurra, C. (2013) An isotopic and modelling study of flow paths and storage in Quaternary calcarenite, SW Australia: implications for speleothem paleoclimate records. Quaternary Science Reviews 64(0), 90-103.

Treble, P.C., Fairchild, I.J., Baker, A., Meredith, K.T., Andersen, M.S., Salmon, S.U., Bradley, C., Wynn, P.M., Hankin, S.I., Wood, A. and McGuire, E. (2016) Roles of forest bioproductivity, transpiration and fire in a nine-year record of cave dripwater chemistry from southwest Australia. Geochimica et Cosmochimica Acta 184, 132-150.

Treble, P.C., Fairchild, I.J., Griffiths, A., Baker, A., Meredith, K.T., Wood, A. and McGuire, E. (2015) Impacts of cave air ventilation and in-cave prior calcite precipitation on Golgotha Cave dripwater chemistry, southwest Australia. Quaternary Science Reviews 127, 61–72.

Williams, P.W. (1983) The role of the subcutaneous zone in karst hydrology. Journal of Hydrology 61(1–3), 45-67.